DISTRIBUTION STATEMENT A. Approved for public release; distribution is unlimited.

Assimilation of Long-Range Lightning Data over the Pacific

Professor Steven Businger Ph.D. (1986)
Meteorology Department
University of Hawaii
2525 Correa Road
Honolulu, HI 96822 USA
Telephone: (808) 956-2569 Fax: (808) 956-2877 email: businger@hawaii.edu

Award No.: N00014-05-1-0551
http://www.soest.hawaii.edu/MET/Faculty/businger/projects/pacnet/
http://www.soest.hawaii.edu/cgi-bin/pacnet/tcs10.pl

LONG-TERM GOALS

A Pacific Lightning Detection Network (PacNet) was designed and constructed with support from ONR, NASA, and Vaisala. In 2009, Vaisala completed an independent and superior network with Northern Hemisphere coverage, Global Lightning Detection (GLD360). The new network benefitted directly from the successes and challenges experienced in developing PacNet. This project aims to support operational utilization of the long-range lightning data stream for (i) nowcasting convective activity, (ii) convective rainfall analyses over the Pacific, and (iii) to improve marine prediction of cyclogenesis of both tropical and extratropical cyclones through sferics data assimilation in NWP models.

OBJECTIVES

The scientific and technical objectives of this project are to collect long-range lightning data over the North Pacific Ocean, refine the relationships between lightning and storm hydrometeor characteristics, and assimilate lightning derived products into operational numerical models. Various assimilation methods will be investigated to find an optimal way to assimilate lightning data operationally into NWP models.

A goal of this project is the development of forecast guidance tools that combine graphics derived from lightning data with other data sets to maximize their utility in short term forecasting of tropical cyclogenesis. Lightning data from PacNet/LLDN or GLD360 will also be combined with data from TCS field operations to investigate the morphology of lightning outbreaks in developing tropical cyclones over the Northwest Pacific Ocean.

APPROACH

Long-range lightning observations provide a means to identify and model under-resolved mesoscale and unresolved storm-scale areas of deep convection over the data-sparse open oceans. Diabatic heating sources, especially latent heat release in deep convective clouds play a central role in storm development and dynamics. Specifying diabatic heating sources in the early hours of the forecast can improve the model's performance.

Real-time Forecast Guidance Tools (Nowcasting Tools)
Data from PacNet/LLDN and GLD 360 are used to develop forecast guidance tools that are available to the forecaster in near real time. The tools combine graphics derived from lightning data with other data sets to maximize their utility in short term forecasting of tropical cyclogenesis.

Assimilation of Lightning Data
We have been investigating three approaches the lightning data assimilation. In the first approach, the lightning data assimilation *(*LDA) method follows the technique described by *Pessi and Businger* [2009b] and utilizes an empirically derived lightning rate-convective rainfall relationship [*Pessi and Businger*, 2009a] described by

$$R = 0.56 * \ln(F) + 8.49, \qquad (1)$$

where R is rainfall rate and F is flash rate per 30 min per (15 km)^2 The coefficient of determination (R^2) is 0.93 . The method was implemented in the Kain-Fritsch convective parameterization scheme by modifying the model-generated vertical heating profiles. The model assigns a certain temperature change to each model level based on the enthalpy difference between liquid and vapor phases of water (latent heat). The method scales the model's vertical latent heating profiles at each grid point and model level depending on the ratio of rainfall predicted by the model to rainfall derived from lightning data.

The Weather Research and Forecast-Advanced Research WRF (WRF-ARW) model is utilized in the first two approaches to our data assimilation. WRF is initialized with 6 hourly Global Forecast System (GFS) analyses, which also provided boundary conditions during the runs. The Lin microphysics scheme is used, which includes ice, snow, and graupel processes. The planetary boundary layer (PBL) scheme used is the Mellor-Yamada-Janjic (MYJ) scheme.

Four simulations were run, which were initialized with: i) a bogus vortex without lightning data, ii) a bogus vortex with lightning data, iii) no bogus vortex nor lightning data, and iv) no bogus vortex with lightning data. The wind profile of the bogus vortex is given by a Rankine vortex with parameters based on the best track information at the time of initialization. The bogus works on the initial data. It is axis-symmetric, has a nearly saturated core, and has mass and wind fields in non-linear balance. The horizontal radius of influence for lightning was set to equal one grid length, i.e., if a flash occurs within the radius of influence from a grid point, it has impact on that point. All lightning data within 600 km of the storm center were assimilated on a 15-km resolution domain during the first 6 hours of the simulation. For the remainder of each simulation an additional storm following (3 km resolution) domain was introduced, where the domain follows the 500-hPa circulation of the typhoon. The 15-km model resolution for the lightning data assimilation (LDA) period was chosen partly because the location accuracy of the lightning data (10-30 km) is reasonably close (1-2 times) to the model grid-length. The Kain-Fritsch convective parameterization scheme was used with the outer, 15-km domain, whereas in the nested 3-km domain, convection was resolved explicitly. The simulation was run for 60 hours, from 1200 UTC 26 September 2008 to 0000 UTC 29 September. According to the best-track data, Jangmi's central pressure dropped from 944 to 933 hPa during the 6-h LDA period. The sustained winds increased from 105 to 120 kt making Jangmi a category 3 storm at the beginning of the LDA period and a category 4 storm at the end of the LDA period. It should be noted that lightning data assimilation may have different impacts at different stages of the TC life cycle. The LDA period

used in this study was chosen because of enhanced lightning activity both in the rainbands and near the storm center.

A second approach to data assimilation that is currently under development employs the Local Analysis and Prediction System (LAPS) to ingest pseudo reflectivity data derived from the lightning rates. The advantage of this approach is that it results in balanced fields for the model.

The LAPS lightning data assimilation method converts the lighting rates from LLDN into vertical radar reflectivity profiles. The profiles are constructed based on results of empirical studies (Pessi and Businger 2009). The profiles are then used to construct a 3-dimensional radar reflectivity grid, which was subsequently ingested by the LAPS cloud analysis package. This approach can be employed in areas where actual radar data are unavailable because of the distance from the nearest radar to the storm is too great.

In the first test of this approach, lightning data from the Long-range Lightning Detection Network (LLDN) were assimilated into LAPS to investigate the impact of lightning data on the intensification and track of hurricane Katrina. The LAPS analysis was then used to initialize the WRF model. The lightning data were assimilated during a 6-hour period between 00 and 06 UTC on 27 September 2005. During that time two lightning outbreaks occurred in the eyewall and Katrina underwent rapidly intensification.

A third approach to the data assimilation is to apply ensemble data assimilation (EnKF) to merge the capabilities of adaptive grid modeling and long-range lightning observations to investigate several aspects of the tropical cyclone life cycle. The proposed methodology involves reading a time series of lightning pseudo-reflectivity fields that can mapped to the adaptive grid within an analysis area centered on the tropical cyclone. During the simulation the model grid spacing will be automatically reduced over the observed locations of the mapped lightning pseudo-reflectivity fields. Ensemble data assimilation will then be employed to assimilate the lightning pseudo-reflectivity observations and nudge the model hydrometeor fields.

Case studies that have been identified for future modeling work include: 1) Formation (Typhoon Hagupit, September 14–18, 2008); 2) Rapid Intensification and Maximum Intensity (Typhoon Megi, October 14–17, 2010); 3) Re-intensification (Typhoon Sinlaku, September 17–20, 2008); 4) Landfall (Typhoon Fanapi, September 17–20, 2010); and 5) Extratropical Transition (Typhoon Malakas, September 24–26, 2010).

WORK COMPLETED

1. Cases of tropical cyclogenesis from TCS-08 and TCS-10 operations period were identified and investigated. Lightning data from all named tropical cyclones during TCS-08 and TCS-10 were used to study the evolution of eyewall lightning and radial distribution of lightning strikes (Fig. 2). For an archive of storm centered imagery see http://www.soest.hawaii.edu/cgi-bin/pacnet/stormcentered.pl . (Team)
2. Operational lightning data tools have been constructed and implemented at the University of Hawaii and are available in real time at http://www.soest.hawaii.edu/cgi-bin/pacnet/tcs10.pl . In addition the graphics were made available to the ITOP data management site. (Pessi, Robinson, and Stolz).

3. WRF model simulations have been run to investigate the impact of lightning data assimilation on Typhoon Jangmi. (Pessi and Chambers)
4. A numerical study was completed on the effects of mesoscale orography on tropical cyclones near Hawaii's Big Island. (Chambers)
5. Work was begun with the OMEGA model to perform idealized and real-case simulations of tropical cyclones as a first step toward developing an efficient method to assimilate lightning observations from Vaisala's Long-range Lightning Detection Network (LLDN) and Global Lightning Dataset (GLD360). This work focused on the development and testing of cloud microphysics and grid adaptation criteria. Other exploratory work involved initializing the model with lightning observations. (Dunn)
6. High resolution (250 m) WRF simulations were conducted of the interaction of deep convection and Oahu's steep windward orography, with a focus on precipitation patterns and the microphysics that accompanies charge separation. (Murphy)
7. GLD360 data from 2010 were compared with TRMM precipitation radar products and the results were compared with the results reported in Pessi and Businger (2008).

RESULTS

Comparison of GLD360 data and TRMM Radar Reflectivity Data

GLD360 data from 2010 were compared with TRMM precipitation radar products and the results were compared with the results reported in Pessi and Businger (2008). For the West Pacific and Atlantic Ocean basins the data are consistent and show an exponential increase in radar reflectivity with increased lightning rate (Fig. 1). In addition, the winter lightning rate correlated to higher radar reflectivity than the summer lightning rate for both basins, and the results show comparable R2 values. These findings are consistent with the previously found relation between lightning and radar reflectivity by Pessi et.al. (2009). The difference between these two studies appears in the maximum reflectivity, which is lower during the PacNet study. Data over the East Pacific are relatively sparse compared to the other basins. Increasing the minimum convective area within a grid box from one pixel to nine TRMM pixels, reduced the number of outliers significantly. By varying the spatial and temporal parameters used to determine the correlation between lightning and radar reflectivity data, the results show that normalized lightning rates are sensitive to the grid-box size and to a less extend to the time-window. Increasing the time-window resulted in larger variability for the normalized lightning rates, and increasing the grid-box size corresponds to a decrease in normalized lightning rates. The greatest sensitivity of radar reflectivity to lightning rate is obtained by using a larger grid-box size and a smaller time-window.

New Nowcasting tools developed

Five tools for displaying lightning data have been developed. These products are available in real time online and were actively utilized during the TCS-10 field experiment. An archive of these products is available and represents a rich resource for future analysis and case study work for TCS-8 and TCS-10.

Graphics have been constructed to show of lightning counts within 50 or 300 km radius, respectively, of the storm center vs storm central sea-level pressure. These graphics are triggered by bulletins issued by the the Joint Typhoon Warning Center (JTWC) (Fig. 2). Lightning bursts after storm's deepest

pressure was reached are associated with the storm making landfall in the Philippines and then outer rainbands interacting with Taiwan (see Figs 3 and 4).

Lightning data were overlaid on satellite imagery to reveal areas of more vigorous convective development in tropical cyclones during TCS-08 and TCS-10 field campaigns. Shades of blue indicate negative charge to ground and red for positive to ground, and the size of the circles gives a measure of the current (Fig. 3). A 15x15˚ storm-centered tile of IR imagery overlaid with lightning data allows for a closer look at areas of interest. Best track data on the location and intensity of developing tropical cyclones from JTWC are used for this purpose (Fig. 3).

A pseudo-reflectivity product was developed for the western Pacific that is linked to the density of lightning flashes (Pessi and Businger 2009a) (Fig. 4). This product has the advantage that it pinpoints areas of enhanced activity, while reducing or eliminating the low-density flashes that have larger location errors associated with very active convective systems. Note the enhanced rainband off the coast of Taiwan. The heavy rain associated with this outbreak led to numerous landslides and some deaths. The assimilation into numerical models of lightning data for events like this has the potential to improve the prediction of the subsequent exceptional orographic rainfall and flooding over Taiwan.

A product was developed to show the motion of lightning-producing storms for the past 12 hours over the western Pacific Ocean. The most recent flashes are colored red, then the colors transition through a rainbow of colors for older flashes, and finally the oldest flashes fade to black (Fig. 5). The graphic allows the forecaster to distinguish at a glance storms that are moving vs stationary, and storm that are intensifying vs weakening.

Finally, a plan-view graphic has been developed to show storm-core lightning density along the storm track (Fig. 6). Separately, lightning strikes within three hundred kilometers and within fifty kilometers of best track are isolated from the GLD360 data set. For the fifty-km range, only the contribution to lightning density from eye wall and core convection is included, whereas flashes further than fifty kilometers of the circulation center are not counted. In other words, the contribution from convection in spiral rain bands is eliminated. Next, an equal-area bin analysis is carried out within the domain to determine the number of lightning strikes per unit area. A triangulated natural point interpolation of the bin analysis is then contoured to produce the density plot. The intensity classification of the tropical cyclone is included with each geo-location of the circulation center and plotted as an overlay on the density plot.

Assimilation of Lightning Data

Results from the first method of lightning data assimilation: Two sets of simulations were run both with and without the WRF bogus vortex. The model simulations with lightning data showed significant changes in the storm structure compared to the runs without lightning data both during, and persisting well after the assimilation period (Figs. 7). The rainbands were generally more realistically simulated with lightning data, and rainfall rates were more realistic (Fig. 7). In the runs with the bogus vortex, the rapid deepening of the storm during the first hours of the simulation was better simulated using lightning data with up to 27 hPa improvement in the pressure forecast (Fig. 8). However, the LDA run started to weaken the storm too early, whereas the control run started to deepen the storm too late. The LDA method increased the size of the eyewall beyond what was observed, because of the lateral expansion of the cyclonic PV tower. The forecast storm track was improved during the first 30 hours of the simulation when LDA was applied.

Adaptive Grid Model
Idealized simulations of tropical cyclone-like vortices were used to investigate and develop model physics and grid adaptation strategies. The simulations were also evaluated for their potential to serve as a tropical cyclone bogus in real-case simulations. The method described by Smith et al. (2006) was used to construct balanced axisymmetric initial conditions.

For real-case simulations, adding resolution to the OMEGA grid at initialization time using point observations of long-range lightning observations was investigated (Fig. 9). While this method offers a pathway to refine the grid locally, and could be developed further to work with a time series of observations, a more efficient technique involving the use of lightning pseudo-reflectivities (Pessi and Businger 2009b) holds more promise and is being explored. To this end, OMEGA's adaptation algorithms were enhanced to automatically refine and coarsen model grid spacing over evolving fields of simulated radar reflectivity in preparation for ingesting observed lightning pseudo-reflectivity fields. Results of grid adaptation to radar reflectivity from a 48-hour simulation of tropical cyclone Megi (2010) are shown in Fig. 10.

Orographic impact and Tropical Cyclones
Tropical cyclones in the West Pacific often interact with significant orographic features before and during landfall (e.g. Taiwan, the Philippines). We have conducted numerical experiments looking at the interaction of hurricanes with a significant obstacle of limited areal extent, the Big Island of Hawaii (Fig. 11).

Our results reveal that changes in steering flow caused by the Big Island can explain observed changes in intensity and track (Figs. 12 and 13). The simulated storm with the Big Island present has a southward displacement as the storm approaches the island from the east. This occurs in a region where the Big Island causes a southward directed steering flow difference (Fig. 12). This southward steering is caused by lower tropospheric flow blocking by the island topography. In contrast as the storm passes west of the Big Island the steering flow difference becomes strongly southwesterly. Since the storm is moving westward, the effect of this steering is to displace the storm to the north. This is apparent west of the Big Island (Fig. 13)

Orographic impact on Tropical Thunderstorms
A numerical study examined a thunderstorm complex that remained nearly stationary over the Ko'olau Mountain Range for more than six hours on 2 April 2006. This event produced flash flooding in many of the low-capacity northeast-facing watersheds of eastern Oahu. A case study was undertaken to better understand the interaction of moist southeast flow with the complex terrain of Oahu. High-resolution numerical simulations of this event employing the WRF-ARW mesoscale model successfully reproduced the observed pattern of precipitation associated with convection anchored by the orography of the Ko'olaus. The WRF simulation showed an environment conducive to charge separation, with ice particles, graupel, and supercooled water coexisting in the mixed phase region, was present throughout the mature phase of the simulated thunderstorm complex (Fig. 14).

The results of the simulations were combined with observations to produce a schematic diagram of the thunderstorm complex (Fig. 15). The convection over Oahu was sustained by a steady flux of moist conditionally unstable air into the Ko'olaus by the easterly flow at the surface. Lifting by the eastern slopes of the Ko'olaus created the ascent needed for the moist low-level air to reach its level of free convection, triggering vigorous convective development and repeat formation of convective cells. Westerly shear of the low level flow was crucial in organizing the convection. The turning of the

environmental winds from easterly near the surface to southeasterly near and above the mountaintop, combined with light winds at mid-levels, resulted in convective updrafts that tilted northwestward with height throughout the lowest 3 km. Weak mid-level winds over the strong low-level shear anchored the lower portion of the convection to the mountains resulting in minimal horizontal cloud motion and a quasi-stationary convective system. The slope of the updrafts had a large component parallel to the axis of the mountain range, which resulted in the main rain shaft of the convective cells extending along the crest of the Ko‘olaus. In addition to determining the pattern of accumulated precipitation, this tilted updraft structure contributed to the longevity of the thunderstorm complex by keeping rainfall and downdrafts separate from the inflow of warm moist air.

The formation of rainfall was complex and involved mixed phase microphysical processes. The vertical advection of condensate originating below the freezing level by vigorous convective updrafts was crucial in the formation and growth of graupel. These graupel particles formed through the freezing of raindrops and grew by riming with supercooled cloud droplets. This process resulted in a substantial amount of frozen precipitation particles and created an environment conducive to charge separation and lightning in the mixed phase region.

IMPACT/APPLICATIONS

1. Operational lightning data tools have been constructed and implemented at the University of Hawaii’s and are available in real time at http://www.soest.hawaii.edu/cgi-bin/pacnet/tcs10.pl . In addition the graphics were made available to the ITOP data management site and are available in an online archive at UH. (Pessi, Robinson, and Stolz).
3. Data assimilation in WRF shows promise for improving rainband precipitation and intensity forecasts for Typhoon Jangmi. Various other assimilation approaches are being developed and tested. (Pessi, Chambers, and Dunn)
4. The orography of Hawaii’s Big Island was shown to impact tropical cyclone tracks through the impact of flow blocking on the steering currents surrounding the island. (Chambers)
5. A method was developed to use the pseudo reflectivity data to increase the grid resolution of an adaptive model grid. (Dunn)
6. High resolution (250 m) WRF simulations over Oahu’s steep windward orography demonstrated that the model was able to resolve the microphysics associated with charge separation and reproduce mountain-scale precipitation patterns associated with terrain anchoring. (Murphy)

TRANSITIONS

The collection of nowcasting tools developed under this award and described above has immediate application in tropical forecasting. We are working with NRL to transition the underlying programs and scripts to allow for quick transition to operations. In addition we are exploring further collaboration to transition data assimilation methodologies.

PUBLICATIONS

Pessi, A. and S. Businger, 2009b: The Impact of Lightning Data Assimilation on a Winter Storm Simulation over the North Pacific Ocean. *Monthly Weather Review,* **137,** 3177–3195.

Pessi, A., and S. Businger, 2009a: Relationships Between Lightning, Precipitation, and Hydrometeor Characteristics over the North Pacific Ocean. *Journal of Applied Meteorology and Climatology,* **48**, 833-848.

Pessi, A., S. Businger, K. L. Cummins, N. W. S. Demetriades, M. Murphy, and B. Pifer, 2008: Development of a Long-Range Lightning Detection Network for the Pacific: Construction, Calibration, and Performance. *Journal of Atmospheric and Oceanic Technology*, **28**, 145-166.

Squires, K. and S. Businger, 2008: The Morphology of Eyewall Lightning Outbreaks in Two Category Five Hurricanes. *Monthly Weather Review*, **136**, 1706–1726.

Murphy, M. and S. Businger, 2010: Orographic Influences on an Oahu Flood. *Mon. Wea. Rev.*, In press.

Chambers, C. R. S., and T. Li, 2011: The effect of Hawai‘i’s Big Island on track and structure of tropical cyclones passing to the south and west. *Mon. Wea. Rev.*, In press.

Pessi, A., C. R. S. Chambers, and S. Businger, 2010: The Evolution of Typhoon Structure with Assimilation of Lightning Data, J. Geophys. Res., in review

HONORS/AWARDS/PRIZES

Dr. Businger was elected Fellow of the AMS in 2010 in part for work accomplished as a result of ONR funding.

FIGURES

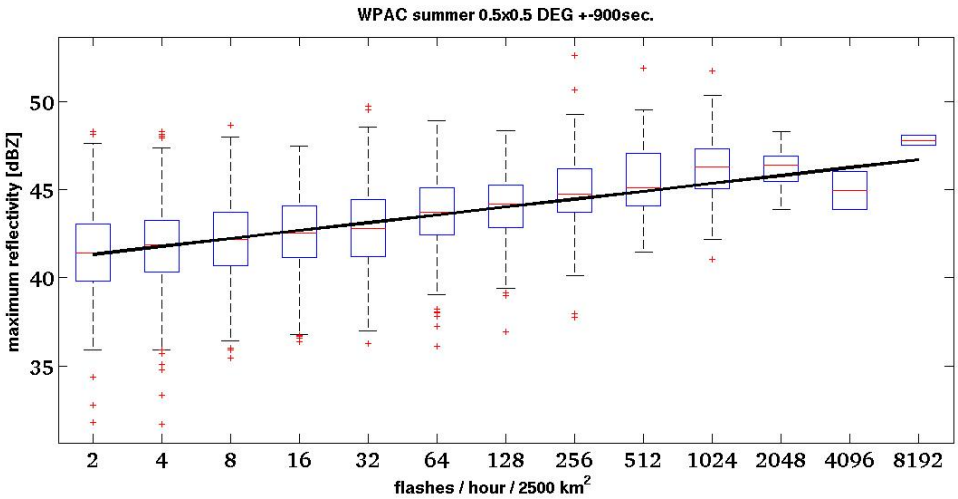

FIG. 1 Maximum radar reflectivity vs. normalized lightning rate over the West Pacific during summer (2010). The box-plots represent the binned lightning data and the solid line is a least square fit on the data. Boxplots show the median (red line), the 25th and 75th percentile (box) and 1.5 IQR (whiskers) for the binned data, the outliers are shown in red. Only grid-boxes with a minimum of 9 out of 16 TRMM pixels flagged convective are included.

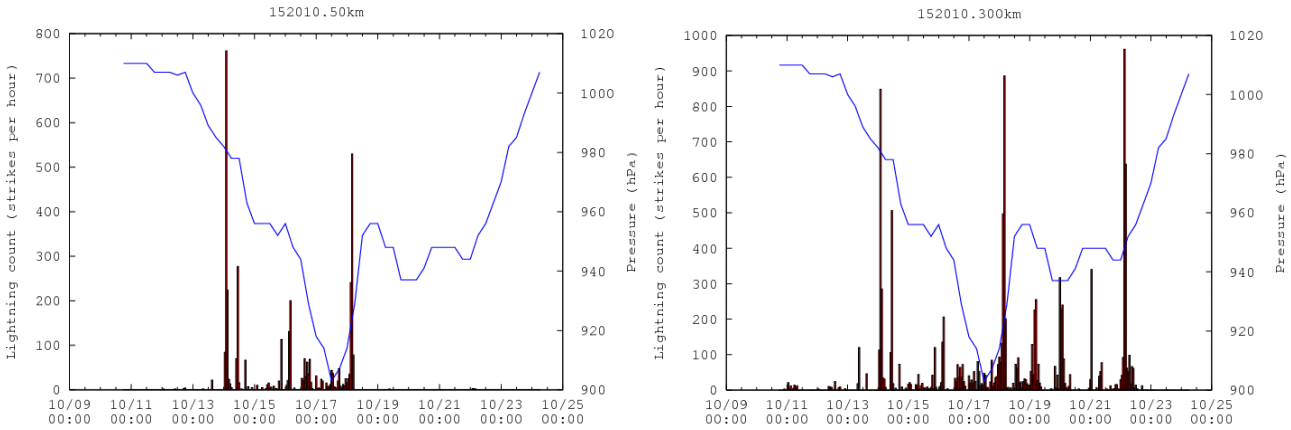

Fig. 2 Graphs of lightning counts within 50 or 300 km radius, respectively, of the storm center vs storm central sea-level pressure for Typhoon Megi.

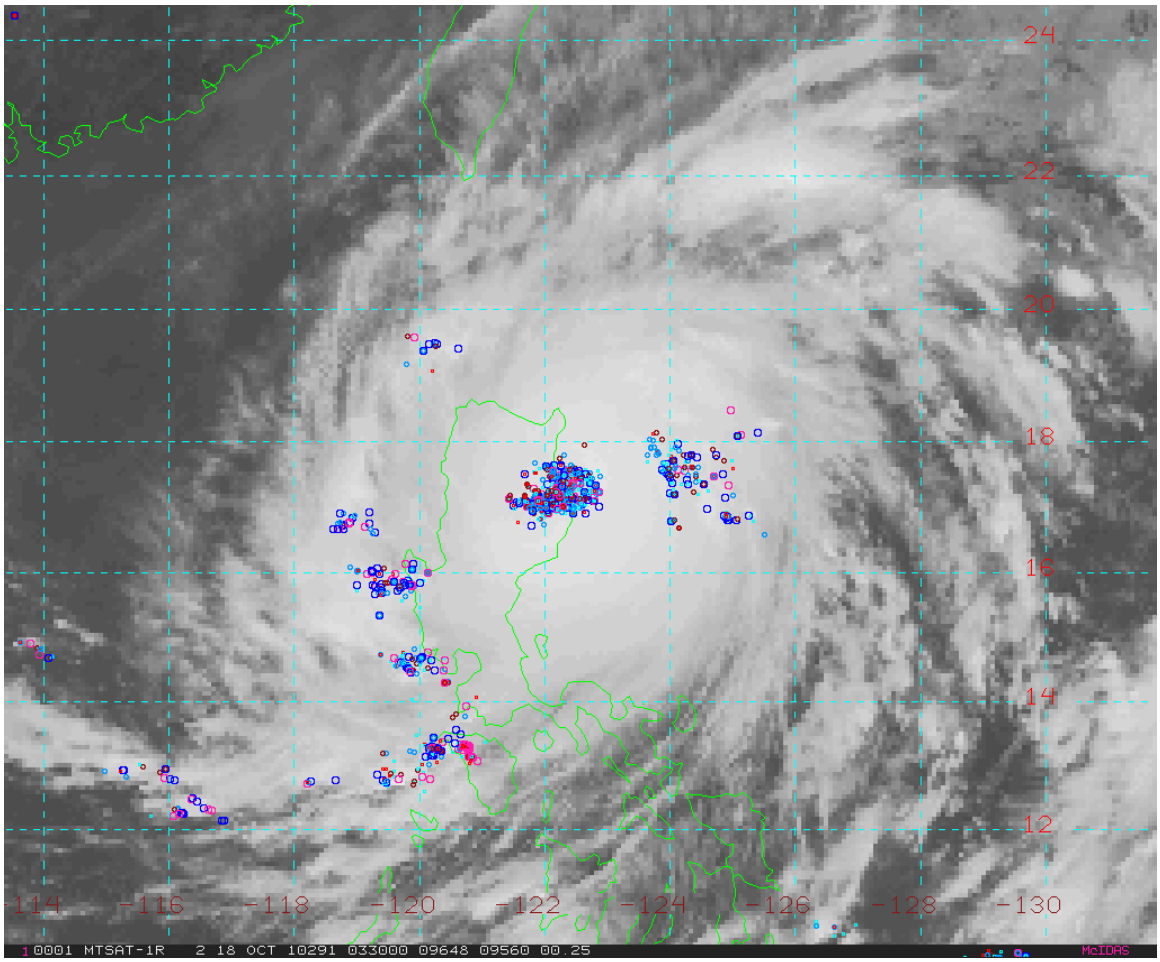

Fig. 3 A concentration of eyewall lightning in Typhoon Megi as it makes landfall on Luzon Island in the Philippines on 18 October 2010. Shades of blue indicate negative charge to ground and red for positive to ground, and the size of the circles reflects the current strength.

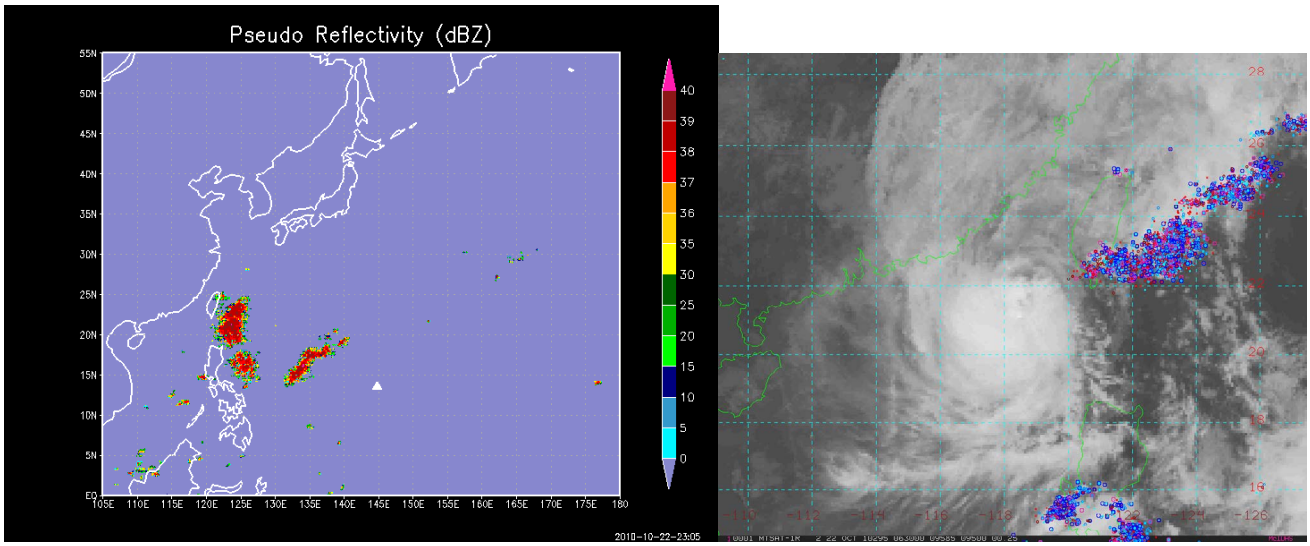

Fig. 4. (Left) Example of a pseudo reflectivity product on 22 October 2010 at 2300 UTC showing estimates of radar reflectivity associated with a rainband from typhoon Megi. (Right) Lightning in vigorous rainband approaching Taiwan. Positive flashes are shown in red shades and negative flashes in blue shades for 0600 UTC, 22 October 2010.

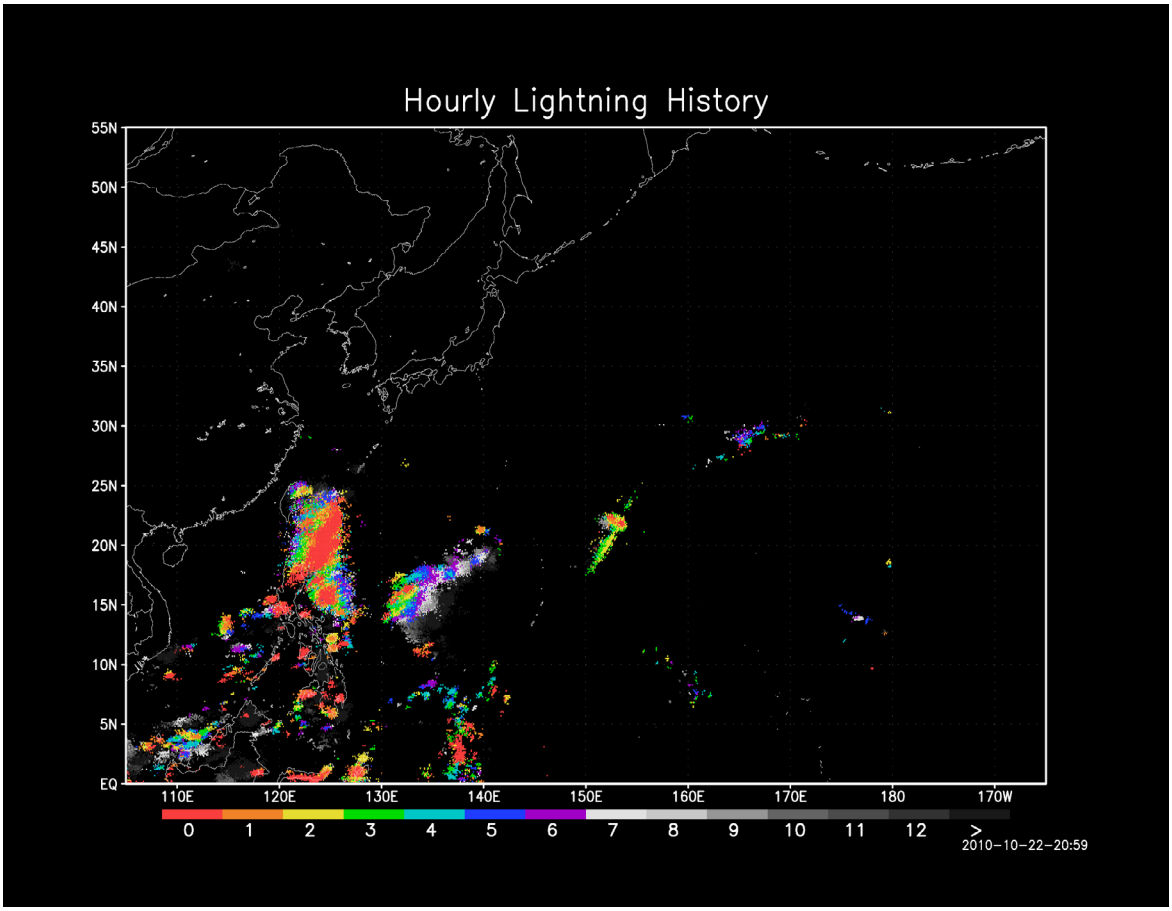

Fig. 5 Image of lightning history associated with Typhoon Megi around the time of landfall. The lightning just east of Taiwan is nearly stationary, and the amount of lightning has increased over the past 2 hours because there is an increase in the orange and red strikes in the image. Meanwhile, the band of lightning further to the east has moved westward over the past several hours.

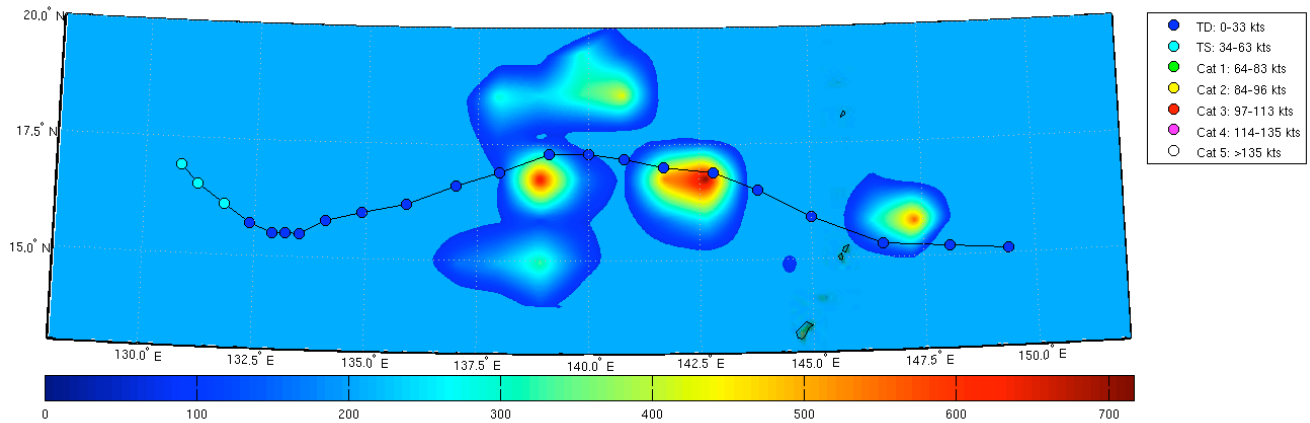

Fig. 6 Two-dimensional graphic showing storm core lightning density along the storm track.

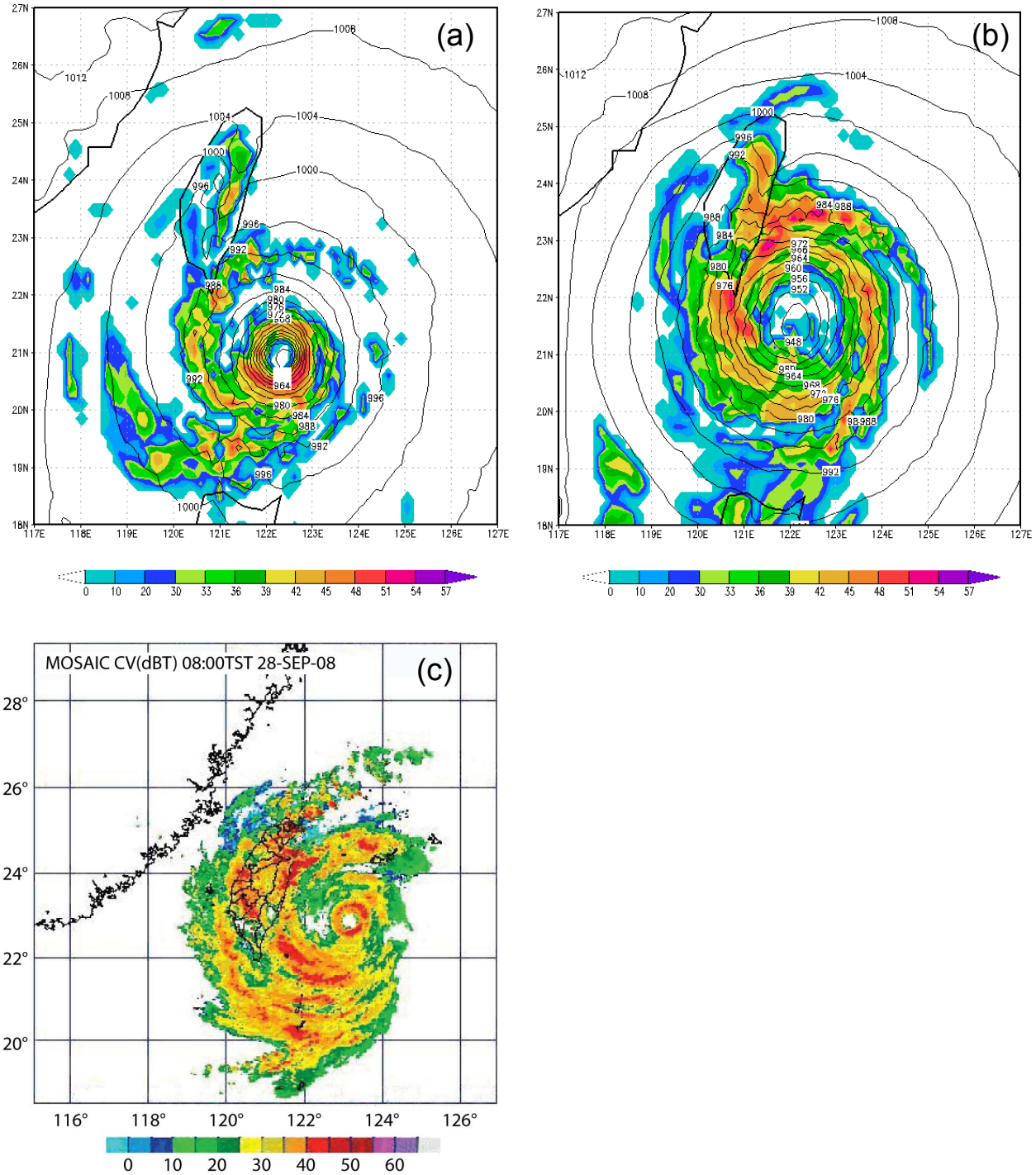

Figure 7. Sea-level pressure (hPa) and simulated radar reflectivity (dBZ) at 0000 UTC 28 September for (a) control and (b) LDA run. (c) Radar image from Taiwan's Central Weather Bureau at the same time.

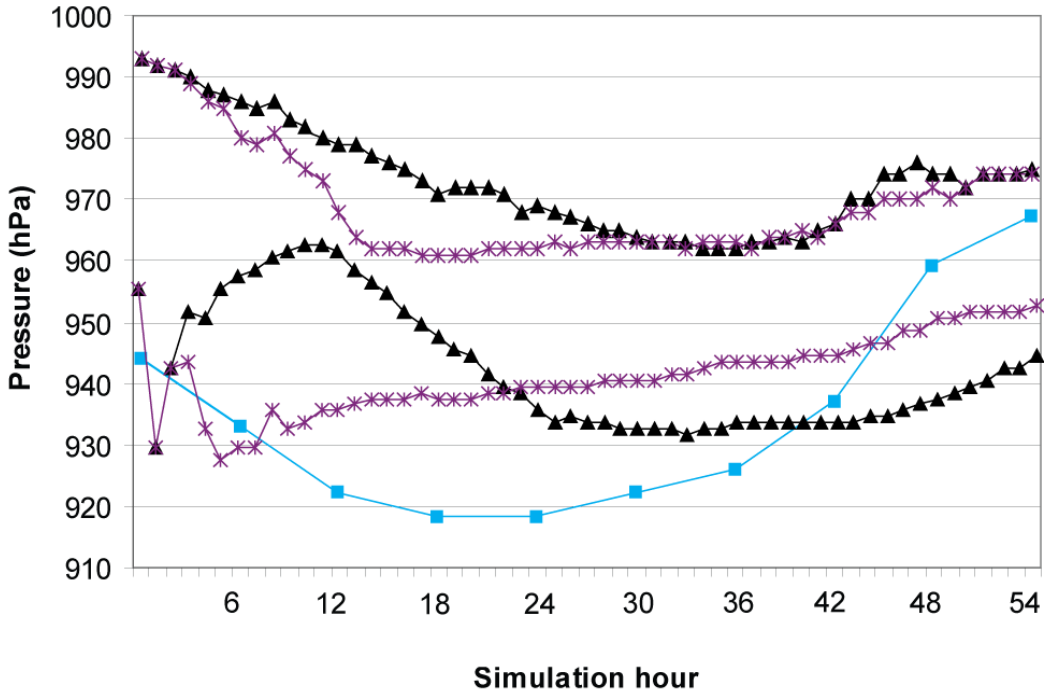

Figure 8. Storm central pressure (hPa) during the simulations without (upper curves) and with a bogus vortex (lower curves) show control run (triangles), LDA (stars), and best track (squares).

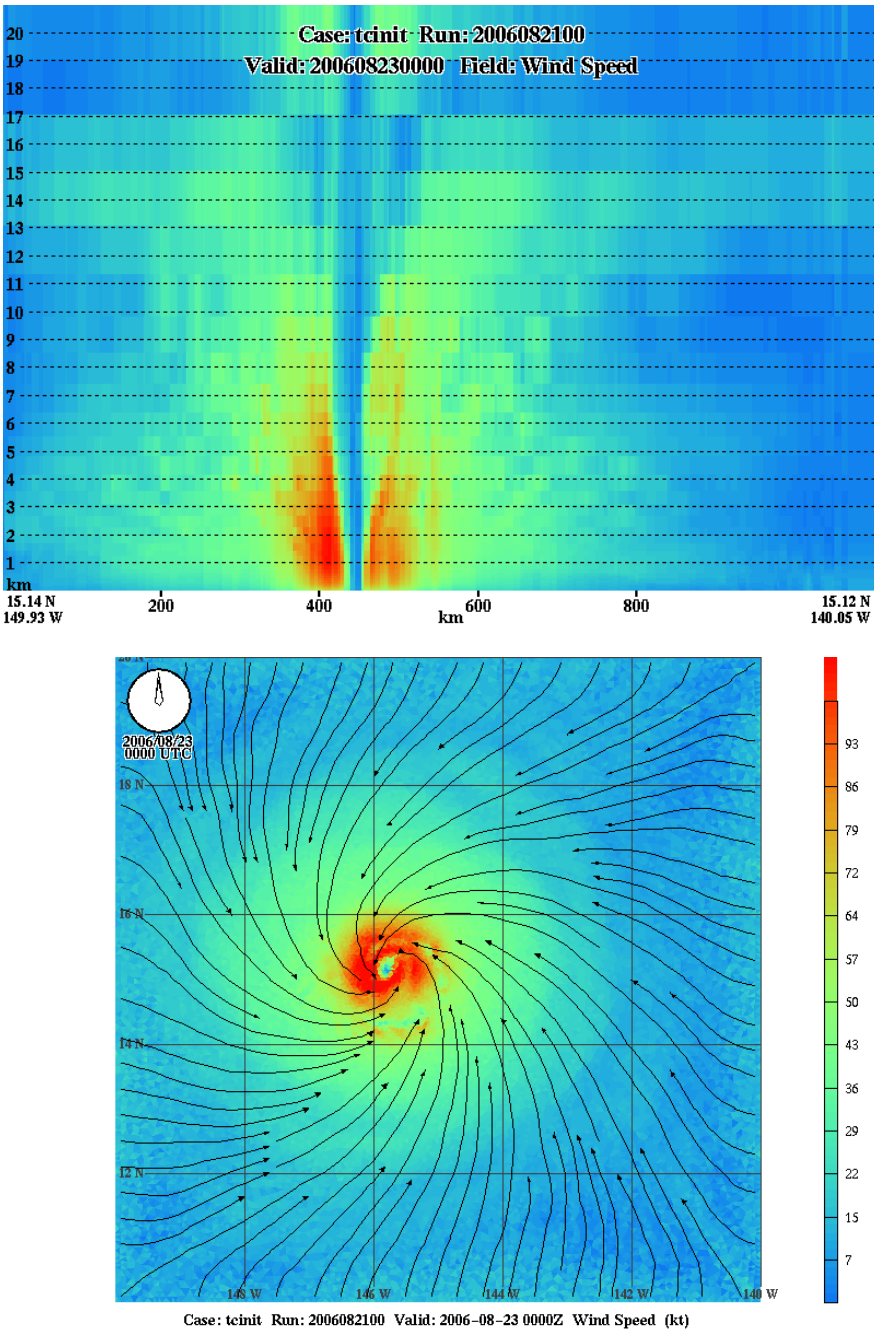

Fig. 9 Results of an idealized simulation starting with a tropical storm perturbation on an otherwise horizontally homogenous environment with constant SST. Cross section (top) and plan view at model level 2 (30 meters) (bottom) of wind speed (knots) at 48 hours.

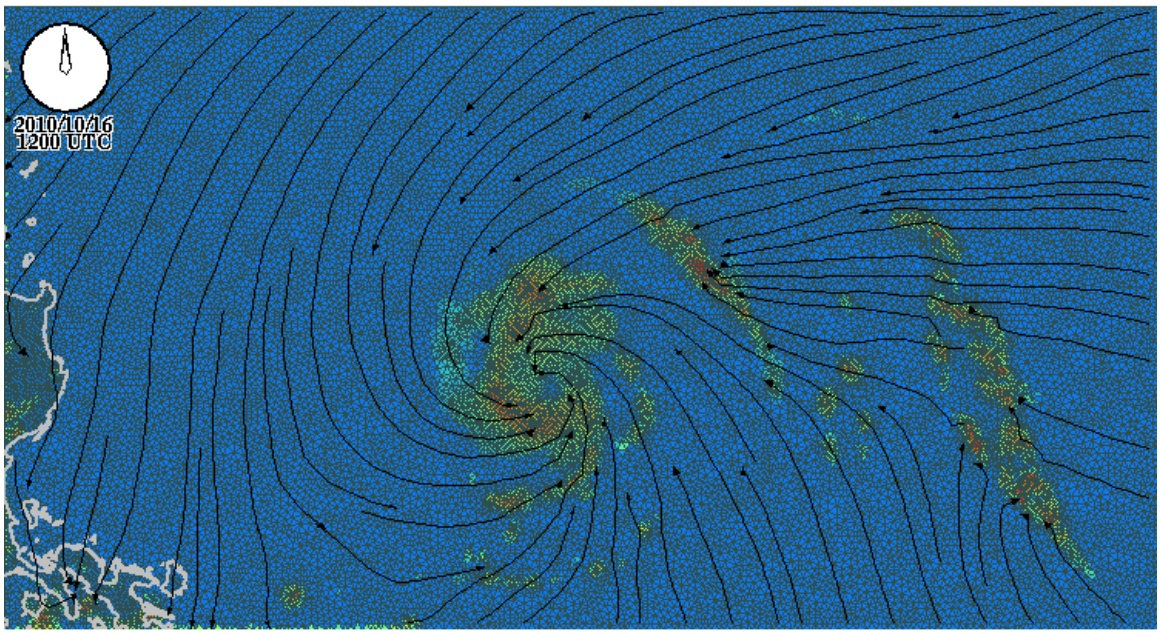

Case: Megi Run: 2010101512 Valid: 2010-10-16 1200Z RRF (dBZ)

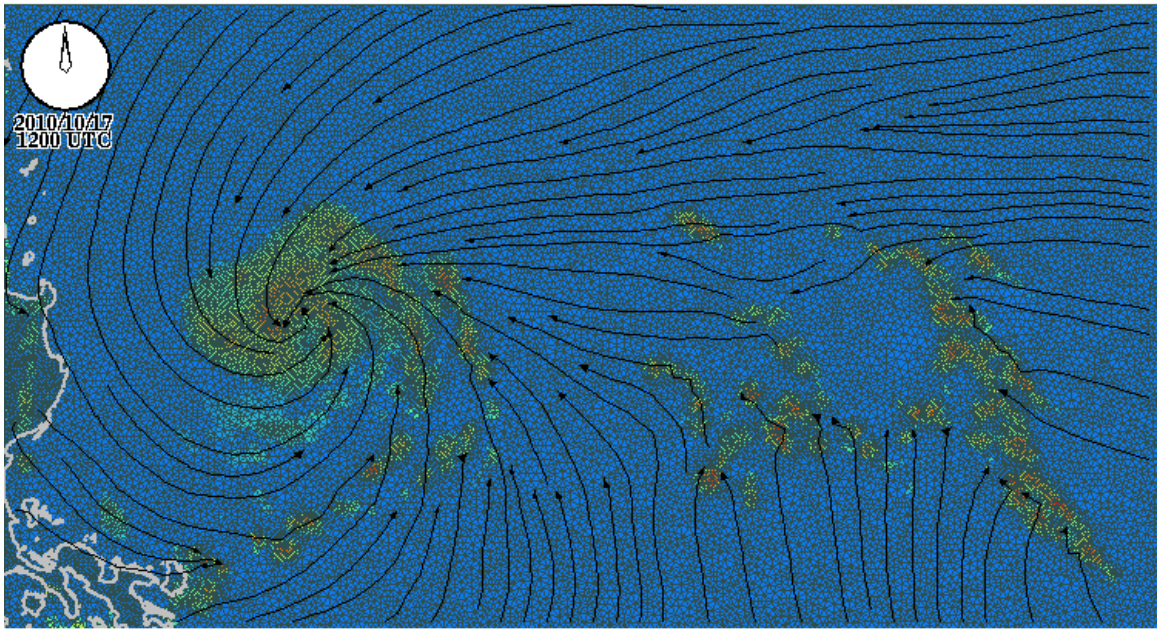

Case: Megi Run: 2010101512 Valid: 2010-10-17 1200Z RRF (dBZ)

Fig. 10 Results of a real-case simulation of Typhoon Megi (2010) at 24 hours (top) and 48 hours (bottom) showing grid spacing automatically increased over evolving fields of simulated radar reflectivity. Grid adaptation is applied to terrain, coastlines, and grid cells with reflectivity > 10 dBZ. The simulation used GFS analysis and 3-hourly boundary conditions. Background grid spacing ranges ~5 to 15 km. Grid spacing under the radar reflectivity fields ranges 3 to 5 km.

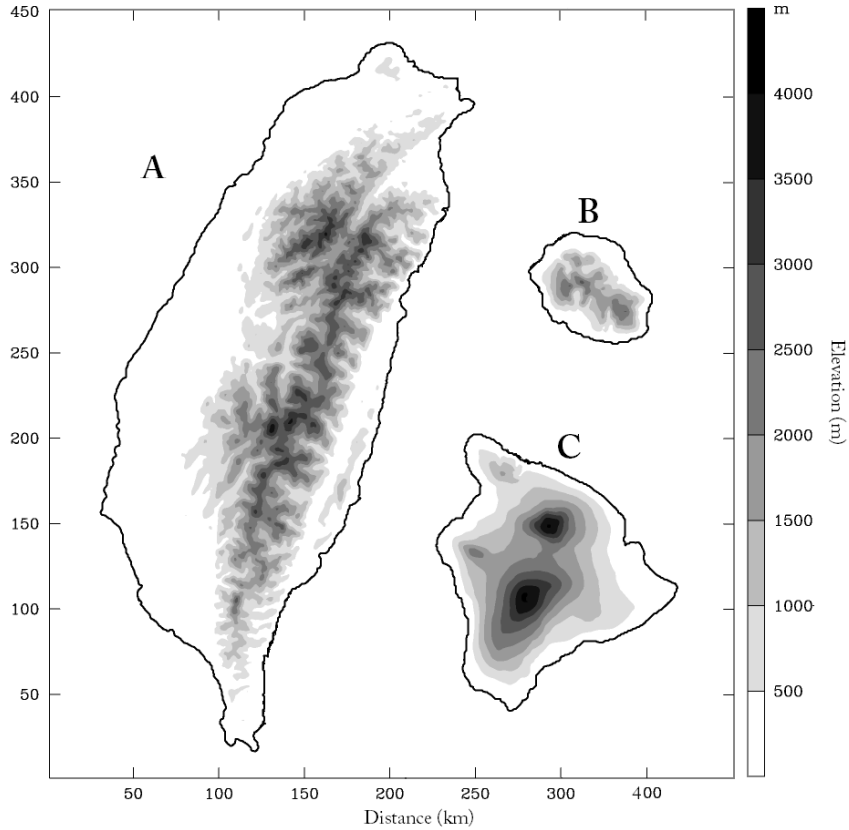

Fig. 11 Topographic maps of A. Taiwan, B. Reunion, and C. the Big Island of Hawaii, shown to scale.

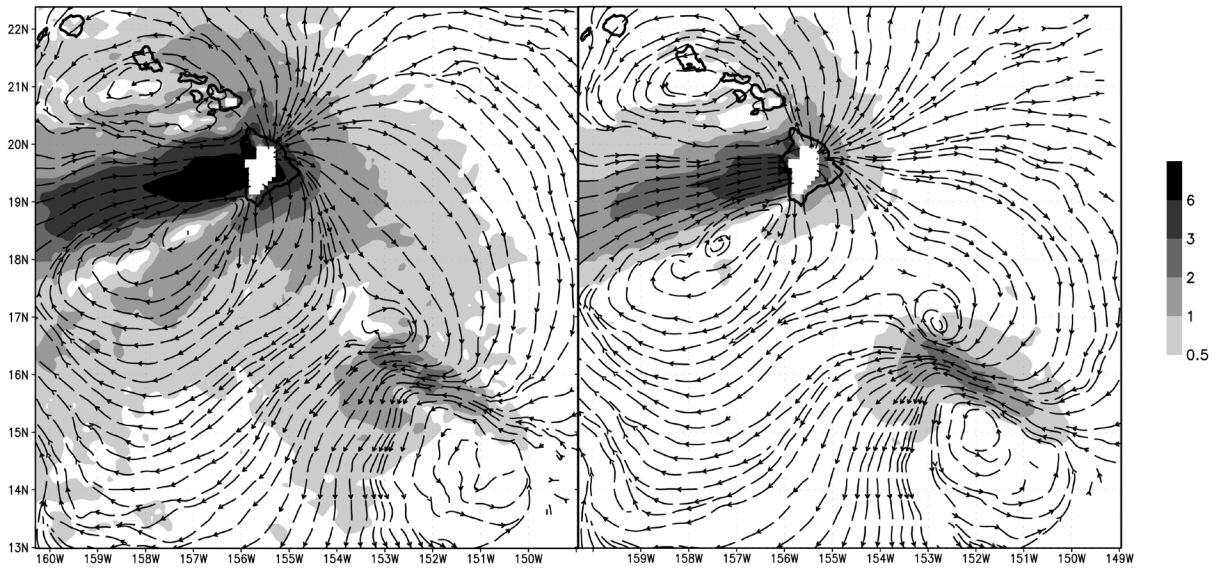

Fig. 12 Tropical storm 850 hPa to 700 hPa (left) and hurricane 850 hPa to 400 hPa (right) steering flow difference (Big Island – no Big Island) in m s^{-1} averaged from hours 12 to 24 for a simulation of Hurricane Flossie (2007).

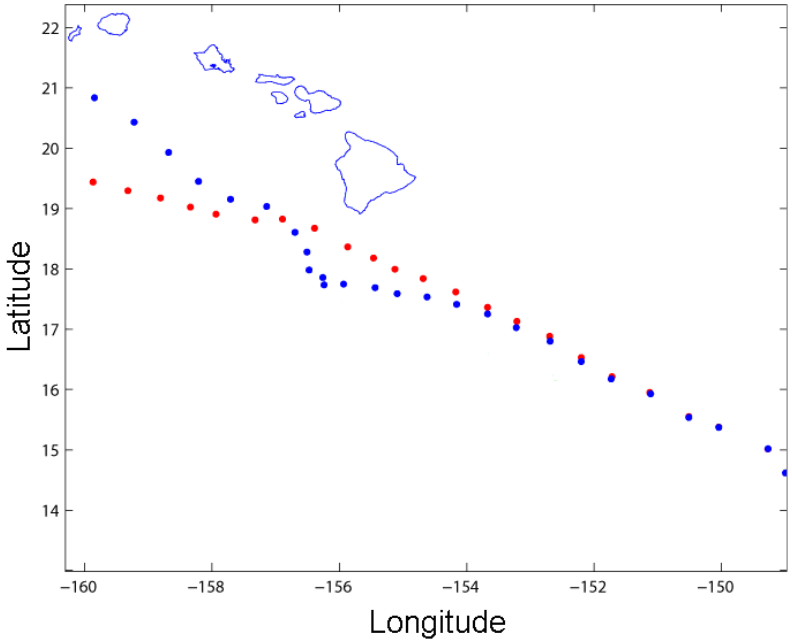

Fig. 13 Simulated tracks with dots every 3 hours for Hurricane Flossie. The track of the blue (red) dots represents the case with (without) the Big Island present.

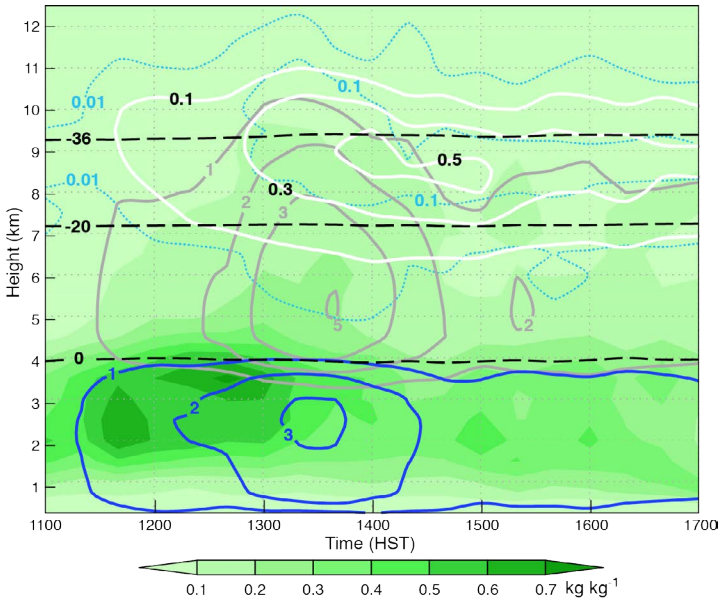

FIG. 14. Time height cross section of rain water mixing ratio (blue contours, kg kg^{-1}), graupel mixing ratio (gray contours, kg kg^{-1}), snow mixing ratio (solid white contours, kg kg^{-1}), cloud liquid water mixing ratio (shaded, kg kg^{-1}), cloud ice mixing ratio (dotted light blue contours, kg kg^{-1}), and isotherms (dashed contours, °C). The values for each hydrometeor are summations over a rectangle encompassing the Ko'olau Mountain Range (158.05-157.7°W and 21.3-21.7°N). Horizontal axis is time (HST) and vertical axis is height (km).

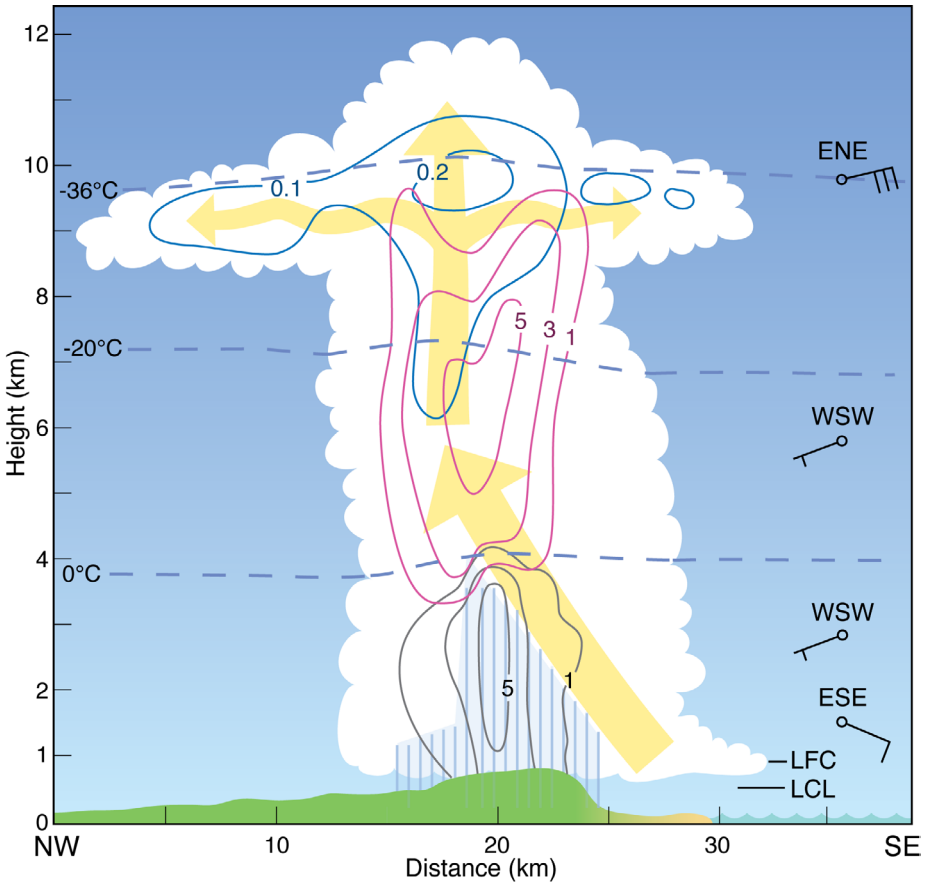

FIG. 15. Conceptual model of a mature convective cell of the 2 April 2006 thunderstorm complex. This schematic diagram displays a southeast to northwest cross section taken through the central Ko'olaus. LCL, LFC, environmental winds, and temperatures are from the Lihue sounding. Rain water mixing ratio (gray contours, g kg^{-1}), graupel mixing ratio (pink contours, g kg^{-1}), snow mixing ratio (blue contours, g kg^{-1}), and cloud circulations (bold arrows) are from the mesoscale model output.